JOURNAL: Mechanical Systems and Signal Processing

Rotating blade vibration analysis using photogrammetry and tracking laser Doppler vibrometry

Benjamin Gwashavanhu

Centre for Asset Integrity Management
Department of Mechanical and Aeronautical Engineering
University of Pretoria
Pretoria
South Africa
Tel: +27 (0)12 420 4762
Cell: +27 (0)74 383 2573
Email: benjigwash@hotmail.co.uk

Abrie J Oberholster

Centre for Asset Integrity Management
Department of Mechanical and Aeronautical Engineering
University of Pretoria
Pretoria
South Africa
Tel: +27 (0)12 420 3288
Cell: +27 (0)83 651 2804
Email: abrie.oberholster@up.ac.za

CORRESPONDING AUTHOR:

P Stephan Heyns

Centre for Asset Integrity Management
Department of Mechanical and Aeronautical Engineering
University of Pretoria
Pretoria
South Africa
Tel: +27 (0)12 420 2432
Cell: +27 (0)82 447 6068
Email: stephan.heyns@up.ac.za

Abstract

Online structural dynamic analysis of turbomachinery blades is conventionally done using contact techniques such as strain gauges for the collection of data. To transfer the captured data from the sensor to the data logging system, installation of telemetry systems is required. This is usually complicated, time consuming and may introduce electrical noise into the data. In addition, contact techniques are intrusive by definition and can introduce significant local mass loading. This affects the integrity of the captured measurements.

Advances in technology now allow for the use of optical non-contact methods to analyse the dynamics of rotating structures. These include photogrammetry and tracking laser Doppler vibrometry (TLDV). Various investigations to establish the integrity of photogrammetry measurements for rotating structures involved a comparison to data captured using accelerometers. Discrepancies that were noticed were attributed to the intrusive nature of the contact measurement technique. As an extended investigation, the presented work focuses on the validation of photogrammetry applied to online turbomachinery blade measurements, using TLDV measurements.

Through a frequency based characterization approach of the dynamics of the two scanning mirrors inside the scanning head of a scanning laser Doppler vibrometer (SLDV), TLDV is employed in developing a system that can be used to achieve a perfect circular scan with a Polytec SLDV, (PSV 300). Photogrammetry out-of-plane displacements of a laser dot focused on a specific point on a rotating blade are compared to displacements captured by the laser scanning system. It is shown that there is good correlation between the two measurement techniques when applied to rotating structures, both in the time and frequency domains. The presence of slight discrepancies between the two techniques after elimination of accelerometer based errors illustrated that the optical system noise floor of photogrammetry does contribute to inconsistences between photogrammetry and other measurement techniques.

Keywords: Photogrammetry; Tracking laser Doppler vibrometry; Non-contact vibration analysis; Turbomachines

1. Introduction

1.1 Turbomachinery vibration measurement

Whilst various techniques such as monitoring the curing process of turbine blades [1] are being employed to improve the quality of manufactured blades, understanding online turbomachinery blade vibrations still remains a matter of great practical importance in the continuous assessment of the condition of rotating structures. This is essentially important for condition monitoring purposes and remaining useful life estimation.

Various measurement techniques can be employed to capture the blade vibration information. Conventionally, contact systems which involve the use of accelerometers and strain gauges are used. These are physically attached to the blades under investigation, and telemetry systems are then used to transfer the measured signals from the transducers to the data logging systems. Even though measurement procedures using these transducers are well established, contact techniques present a number of drawbacks especially when it comes to rotating structures. They are point-wise in nature and only specific blade locations, on a limited number of blades, can be instrumented [2]. Thus vibration response measurements on all blades cannot be captured simultaneously. Being contact in nature, the instrumentation also influences the dynamic behaviour of the system under investigation,

leading to inaccurate measurements. Depending on the material properties of the turbomachine, mass loading effects and local stiffness alterations at the point of transducer attachment can both be sources of errors in captured measurements. The telemetry systems used with these contact techniques are not only costly and time consuming to install [2], but they can also contribute to the electrical noise in the signals from the transducers.

Blade tip timing [2–4] and casing pressure measurements [5] have been employed as non-contact techniques for blade vibration analysis. These techniques are more reliable than contact techniques in terms of life expectancy under the very hostile conditions of high temperatures and pressures under which turbine blades operate [2]. However, they are based on very limited information essentially obtained in the region of the blade tips only, and are subject to potentially large faults in the interpretation of the measured results.

Optical non-contact techniques that allow extraction of vibrational information over the entire blade surface have been proposed. These include laser Doppler vibrometry (LDV) and photogrammetry. In addition to being non-intrusive, these techniques are capable of simultaneously capturing full-field measurements in more than a single degree of freedom (photogrammetry in this case). These techniques are not as well established as the contact techniques, thus there is a need for detailed laboratory investigations to validate them. Superior approaches that can provide deeper physical insight into the nature of blade vibrations of online systems can then be developed for improved condition monitoring practices.

The work presented here uses LDV to validate a form of photogrammetry (3-dimensional point tracking, 3DPT). Good correlation between the two optical non-contact measurement techniques is demonstrated.

1.2 Optical non-contact vibration analysis techniques

1.2.1 Photogrammetry

Photogrammetry is a non-contact full-field measurement technique in which a pair of digital cameras is used to synchronously capture a series of images of the structure under examination. By positioning the two cameras at a known distance from each other, stereo photographs of the object can be obtained which, when viewed together, provide a 3D representation of the object. In the captured image sequence, correlation algorithms are used to track a specific pixel with a particular gray scale value on the surface of the structure [6]. Thus displacement profiles can be obtained through 3DPT of distinct markers attached to the surface of a structure. This can be achieved using photogrammetry software such as PONTOS^{TM} developed by GOM. Furthermore, surface strain distributions can be obtained through digital image correlation (DIC), if a random speckle pattern is applied on the surface [6]. The concepts of image matching for correlation purposes and imaging considerations which include considering the desired depth of field, camera selection and setting of the exposure time, and the basic theory of stereo-photogrammetry are well documented [7,8].

Certain camera parameters have to be established before measurements can be captured using DIC and 3DPT. These parameters are obtained through a calibration process performed using a calibration target. Typically, a standard calibration panel which contains white markers on a black background can be used. The calibration is conducted through tilting and rotation of the calibration target in the volume of space where the structure under investigation will be positioned, while capturing views from different perspectives using the cameras. Through a computation done by the photogrammetry

software, the intrinsic and extrinsic parameters of the camera can be obtained. The intrinsic parameters include the image centre, image skew and the distortion parameters. Extrinsic parameters include the pinhole locations of the cameras and the orientations of the cameras relative to the target. These parameters are needed for the accurate determination of point displacements and structural deformations.

Photogrammetry has been used for the dynamic analysis of turbomachines in work done by other authors [9–14]. A 3D photogrammetric image correlation algorithm based on the Newton-Raphson method has been used to show that the non-contact technique can be used to provide necessary information for early stage damage detection in wind turbines [15]. An investigation into the feasibility of using photogrammetry to monitor large scale wind turbines through the estimation of system dynamic properties has been conducted [14,16]. The initial results from this study indicated that recent advances in hardware and photo-based sensor technology can lead to the replacement of conventional techniques such as using strain gauges. By using the consistency of the recorded data as error estimates, these authors were able to achieve an average accuracy of ±25 mm from a measurement distance of 220 m on a 2.5 MW - 80 m diameter wind turbine.

Dynamic point tracking through photogrammetry has also been successfully used to analyse helicopter rotors [17]. An operational modal analysis was conducted, and the measured data indicated that for the rotors, harmonics of the blade passage frequency dominated the blade responses. In a similar investigation Lundstrom et al. [18] collected operational data of the rotor of a Robinson R44 helicopter, and managed to prove that 3DPT stereo photogrammetry is a robust measurement technique for analysing small rotating structures. Olson et al. [19] successfully demonstrated the ability of stereo photogrammetry to capture blade deflections of a full scale UH-60 rotor whilst actual flight conditions were being simulated in a wind tunnel. In these applications, the measurements captured for the rotating structures were not validated with other measurement techniques.

Zappa et al. [20] performed an uncertainty assessment of DIC for general dynamic applications. The blurring effect that results from target motion can introduce uncertainties in the captured data, unless a sufficiently high frame rate is used. A numerical technique was used to simulate this motion effect on a reference image, and a validation of this technique was done through harmonic excitation of a target. The authors were able to present a method that can be used to quantify the uncertainty induced in the DIC dynamic measurements due to target motion. Using the same technique, DIC performances could be improved by reducing the bias error and uncertainty of the dynamic measurements.

Various approaches have been proposed to improve the robustness and the applicability of the technique to more practical situations. A modal expansion approach which can be used to extract full-field strain data through transformation of point-wise captured measurements to all degrees of freedom of a finite element model, has been successfully developed [11]. This makes it possible for full-field measurements to be obtained even if there are a finite number of measurement points (e.g. due to a limited line of sight of the structure under investigation). A surface stitching technique to combine images captured along different sections of a statically loaded blade have been used to localize damage along a wind turbine blade [10]. Through the use of mirrors, a single camera has been successfully used to capture torsional vibrations in a rotating shaft [21].

Helfrick et al. [22] also used photogrammetry to capture the out-of-plane motion of rotating blades, and illustrated that the approach can be used to capture operational deflection shapes (ODSs). They analysed the dynamics of a small desk fan, and managed to use DIC to capture strain distributions on the surfaces of the fan blades. In addition to capturing the ODSs, they were also able to determine the out-of-plane displacements as a function of the rotation angle. In their work, results were not validated through comparison to other techniques. As an extended investigation to this work, Warren et al. [23]

quantified the performance of photogrammetry by investigating a 1.17 m diameter rotating wind turbine. Two investigations were conducted. In the first investigation, electromagnetic shakers were used to excite the blades in a non-rotating approach to correlate 3DPT and LDV. Good correlation between mode shapes was obtained with Modal Assurance Criterion (MAC) values as high as 99.3%. In the other investigation the correlation between 3DPT and accelerometers was investigated when the turbine blades were being rotated at approximately 10 Hz. Inconsistences were observed between the two techniques. These were attributed to the intrusive nature of the contact method, the cross-axis sensitivities of accelerometers, differences in measurement systems noise floors, and also the noise from the telemetry system. To better investigate the performance of photogrammetry, another optical non-contact technique, TLDV, is employed in this study.

1.2.2 Laser Doppler vibrometry

LDV has been successfully used to investigate dynamic properties of various structures [24]. In applications involving turbomachinery blades, LDV can either be used from an Eulerian or a Lagrangian reference frame. In the Eulerian approach the laser beam is focused at a fixed point in space and the blades sweep through the laser beam as they rotate. Although this approach presents some challenges with regards to signal processing, procedures have been proposed to successfully analyse the data for online blade condition monitoring [25,26].

In the Lagrangian approach the laser beam is steered to follow a specific point on a blade as it rotates. This can be accomplished through a purely mechanical implementation such as self-tracking laser Doppler vibrometry (STLDV) [27]. While there are no rotational speed limitations with STLDV, two additional mirrors are required, and sufficiently accurate alignment of the system becomes challenging.

Instead of using a STLDV system, the capabilities of a scanning laser vibrometer could also be exploited. Harmonic driving signals could be used to simultaneously actuate the two orthogonally mounted mirrors in the scanning head of the LDV. The frequency of these signals corresponds to the rotational scanning frequency of the laser beam. If the rotational scanning frequency of the laser beam is synchronized to that of the rotor, continuous out-of-plane displacements of a single point on a blade can be captured over full rotations. This approach is generally known as TLDV. To obtain perfect circular scans using a scanning LDV however requires characterization of the dynamics of the two mirrors in the scanning head. The reasons for this are that the physical locations as well as inertial properties of these mirrors are not identical [27].

Relationships for the harmonic driving signals that are required for the laser light on the target to follow a circular pattern have been established [28] and are given in Equations (1) and (2).

$$\theta_{s_x} = -\varphi_{s_x}\cos(\Omega_s t + \phi_s) \tag{1}$$

$$\theta_{s_y} = \varphi_{s_y}\cos(\Omega_s t + \phi_s) \tag{2}$$

For a circular scanning frequency Ω_s (in Hz) the time dependent drive signal to the X-mirror is given by θ_{s_x} and that to the Y-mirror by θ_{s_y}. A phase correction in the two signals ϕ_s might also be necessary to obtain a perfectly circular scan. The amplitudes of the driving signals for the X- and Y-mirrors are given by φ_{s_x} and φ_{s_y} respectively. These voltage amplitudes take account of the fact that the two mirrors are at unequal distances from the target, and are also dependent on the circular scanning radius of interest r_s, the distance between the scanning mirrors d_s, and the distance of the

mirrors to the measurement plane z_0. To determine the actuating signal amplitudes, Equations (3) and (4) can be used [28].

$$\varphi_{s_x}(t) = 0.5 \tan^{-1}\left(\frac{r_s}{z_0 + d_s}\right) \tag{3}$$

$$\varphi_{s_y}(t) = 0.5 \tan^{-1}\left(\frac{r_s}{z_0}\right) \tag{4}$$

2. Characterization of the dynamics of the scanning mirrors for TLDV

2.1 Method and Test Setup

At high scanning frequencies, the scanning circular path distorts into an ellipse due to the inertial effects of scanning mirrors and response delays in the scanning system's drive components [29]. An investigation was conducted to characterize the dynamics of the mirrors. Sine sweep signals with a frequency range of 0-20 Hz were supplied to the mirrors, and as the laser dot which was focused on a black painted glass panel rotated, images of the dot were captured using a GOM 4M stereo videography system. With a maximum frame rate capability of 450 frames per second (FPS), the cameras were set to record at 450 FPS when measuring the dot motion. Voltages supplied to the scanning mirrors when the cameras were capturing images were recorded. The corresponding coordinates of the laser dot on the glass panel were also recorded using PONTOS. Figure 1 shows the experimental setup used.

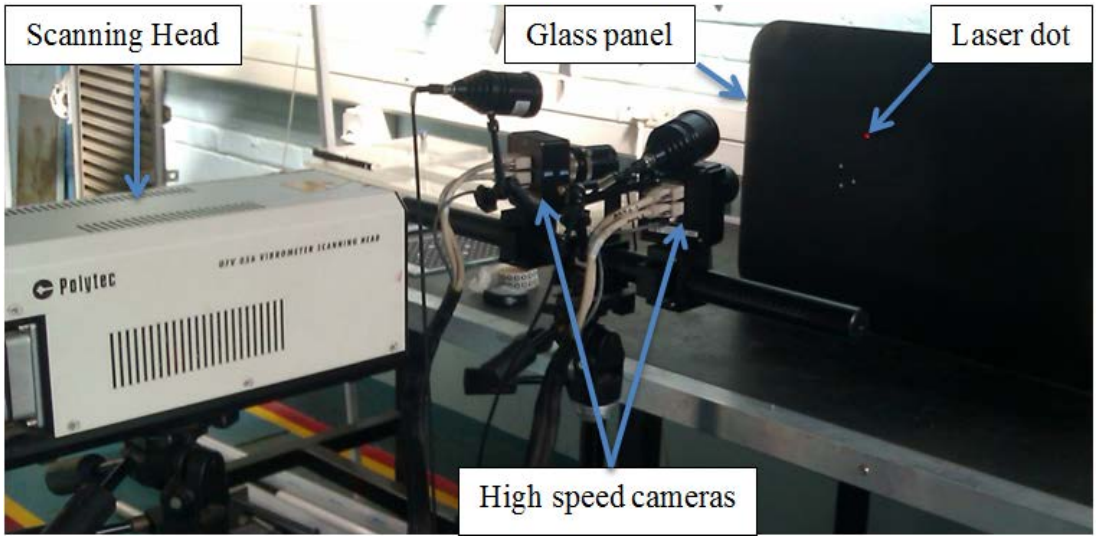

Figure 1: Dynamics of scanning mirrors experimental setup

It is important that the scanning head be as well aligned to the glass panel as possible before images of the scanning path can be captured. An angular misalignment between the vibrometer scanning head and the glass panel can also result in an elliptical scanning path. Whilst perfect alignment is practically impossible, an acceptable system can be obtained by ensuring that the scanning head is horizontal along its length and its width. This can be done by checking the bubble levels on a tripod stand supporting the head. For a perfectly vertical glass panel, ensuring that the two vertical front edges of the scanning head are at the same normal distance from the glass panel will minimize this angular misalignment as well.

After aligning the system, two voltage signals were then used to excite the mirrors. The X- and Y-coordinate positions of the laser dot captured using 3DPT were considered the responses of the scanning mirrors to this excitation. Frequency response functions (FRFs) of the mirrors to voltage

excitations could then be determined. A frequency resolution of 0.205 Hz was specified, as determined from the time increment of the input time history signals. Results obtained from this frequency response analysis were used to perform a phase and amplitude compensation to improve the scanning paths.

The distortion of the circular scanning path, with increasing scanning frequency (5 Hz to 40 Hz) is illustrated in Figure 2 for the Polytec 300 scanning laser vibrometer that was used in this investigation. Also shown in the figure are circularity constants C_c, determined using Equation (5).

$$C_c = \frac{4\pi A}{P^2} \tag{5}$$

In Equation (5), A is the area of a polygon estimated using the Matlab polyarea.m function and P the perimeter of the scanning path determined through the summation of the lengths of the edges of the scanning paths. The closer C_c is to unity the better the scanning path approximates a perfect circle. Thus a perfect circle will have a C_c equal to unity and as the scanning path becomes increasingly elongated, C_c approaches zero.

It therefore becomes necessary that the actuating signals suggested in reference [28] be modified to account for dynamics of the scanning mirrors to obtain a perfectly circular scan.

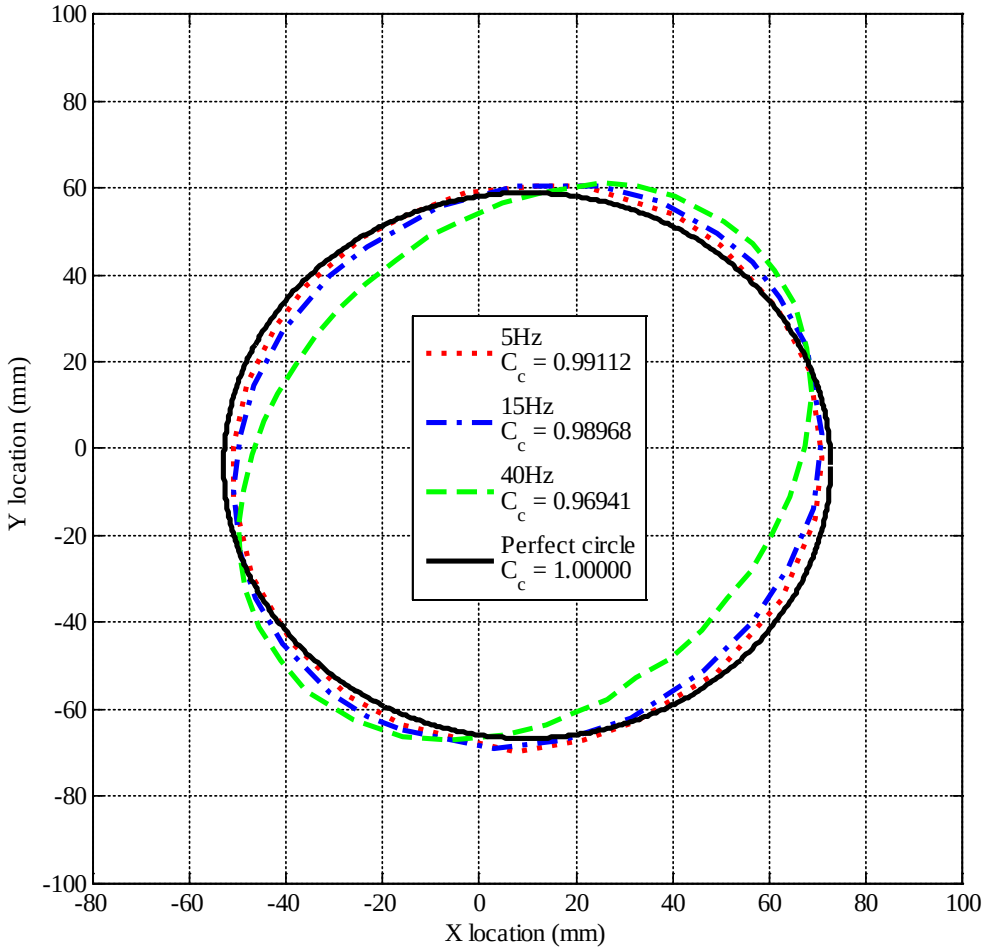

Figure 2: Variation of circular scanning path with frequency

2.2 Results and discussion

Figures 3 shows the phase response functions obtained for the X- and Y-mirror dynamic characterization.

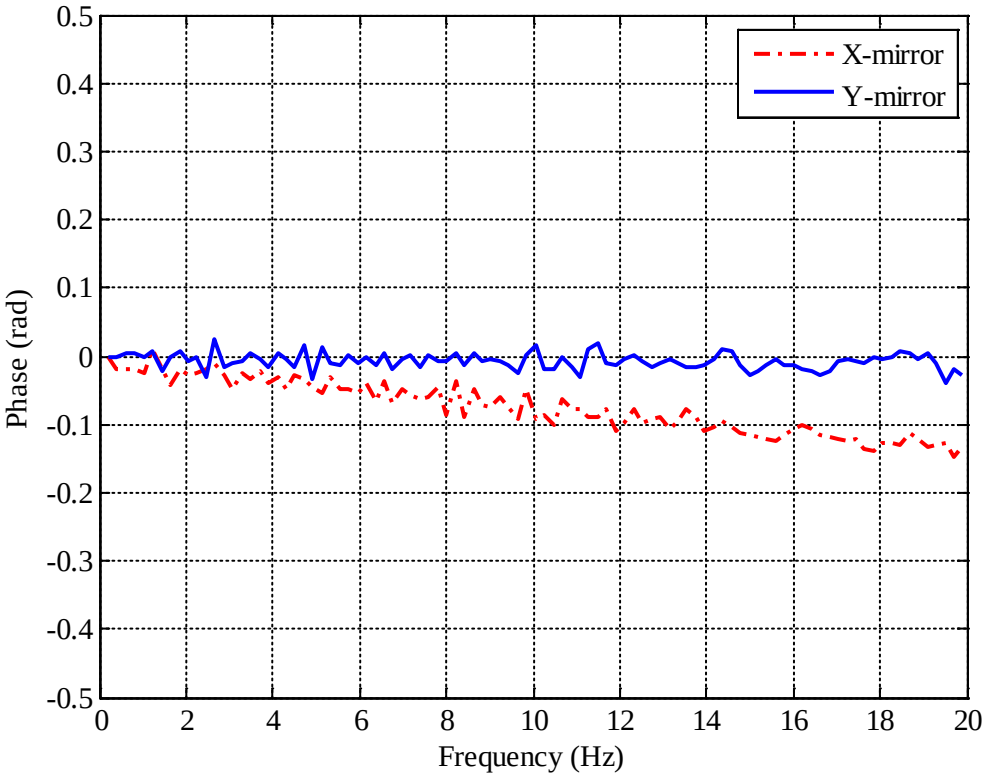

Figure 3: Mirror phase response function (0-20 Hz frequency sweep)

From Figure 3, a phase lag for the X- scanning mirror with the increase of rotational frequency from 0 Hz to 20 Hz can be observed. Over the frequency range considered, the phase lag changes linearly with the frequency. A least squares linear fit was used to determine a relationship that could be used to calculate the phase compensation ϕ_s, for the X-mirror for a particular frequency of rotation ω in Hz, as required in Equation (6).

$$\phi_s = -6.597 \times 10^{-3}\omega - 8.802 \times 10^{-3}\, rad \tag{6}$$

To check for consistency in the determined relationship, 0-10 Hz and 0-15 Hz frequency sweeps were also performed, and Figure 4 shows results of the different relationships for each sweep considered for a rotational frequency range, ω, 0:20 Hz. The figure indicates that consistent results are obtained for the different frequency sweeps investigated, with a maximum phase lag difference of about 0.0023 rad at 0 Hz between the 0-10 Hz and the 0-20 Hz frequency sweeps.

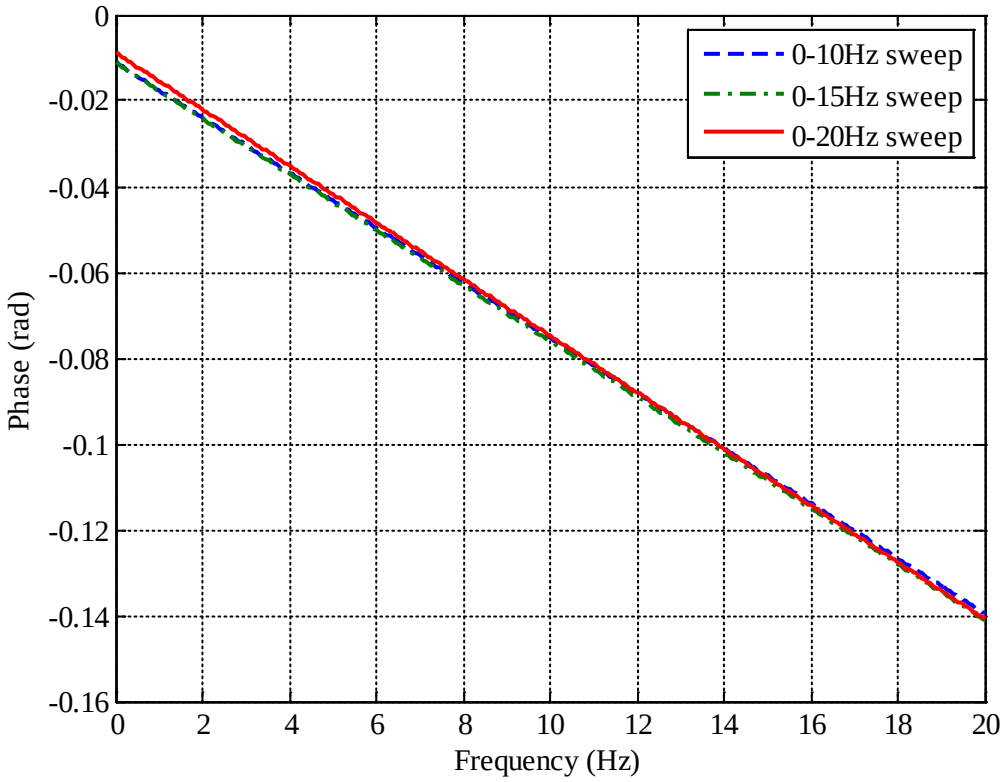

Figure 4: Phase response functions for the X-mirror for different sweeps

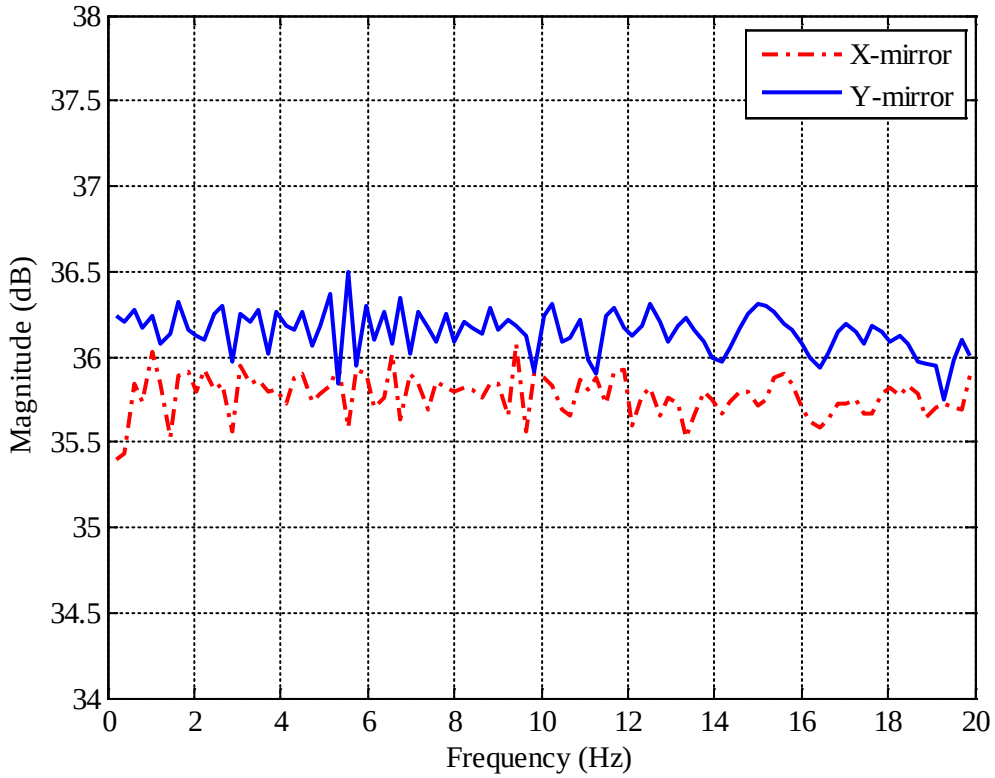

Figure 5: Mirror magnitude response function (0-20 Hz frequency sweep)

It is observed from Figure 5 that for both mirrors the magnitude remains essentially constant with frequency. In addition, excitation of both mirrors using signals of identical amplitudes results in the X-mirror having a FRF magnitude that is less than that of the Y-mirror by an average factor of 1.05879. Considering the fact that the X-mirror is physically larger than the Y-mirror, it is expected that more energy will be required to rotate the X-mirror by a particular angle than is needed to rotate the Y-mirror by the same angle. Thus for the X-mirror, instead of using Equation (3) to calculate the amplitude of the actuating voltage signal, Equation (7) obtained by multiplying Equation (3) by 1.05879 was used.

$$\varphi_{s_x}(t) = 0.5294 \tan^{-1}\left(\frac{r_s}{z_0 + d_s}\right) \tag{7}$$

Figures 6 and 7 show the results obtained when both amplitude and phase were compensated for, at frequencies of 25 Hz and 40 Hz respectively. Despite the characterization having been performed for only up to 20 Hz, the applicability of the determined compensation parameters was investigated for even higher frequencies.

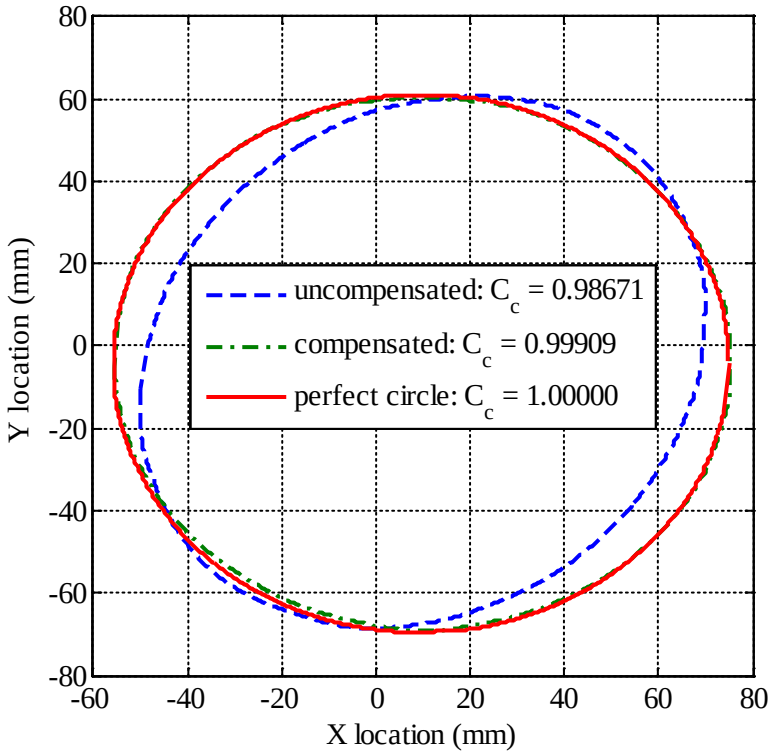

Figure 6: Scanning profiles (25 Hz)

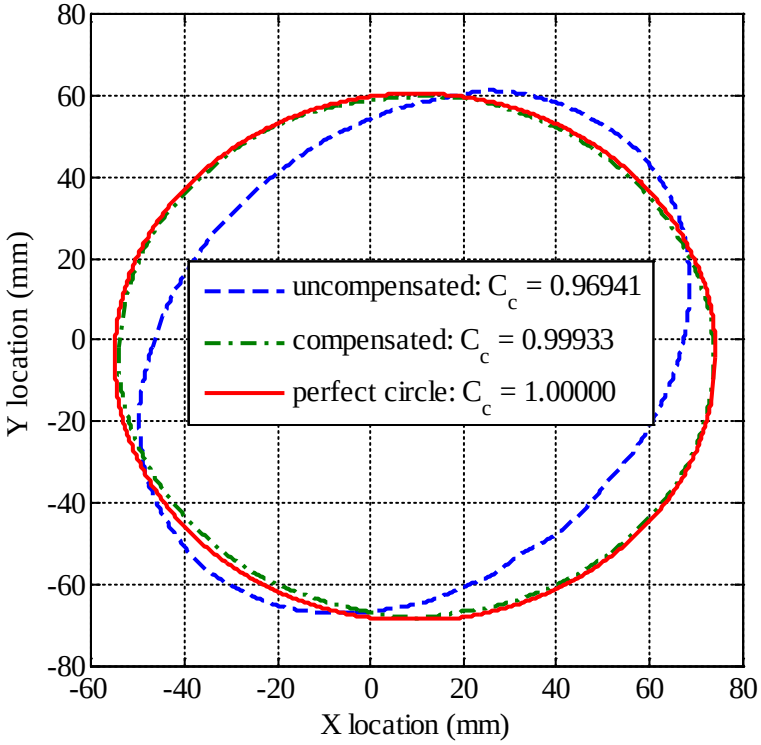

Figure 7: Scanning profiles (40 Hz)

The results from Figures 6 and 7 indicate that the compensated scanning path approximates the perfect circle much better, and for the two scanning frequencies considered, visually the scanning paths are very close to perfect circles. Table 1 shows how the compensation reduces the circularity constant percentage errors.

Table 1: Effect of signal amplitude and phase compensation on circularity constant percentage error

Scanning frequency	Uncompensated percentage error (%)	Compensated percentage error (%)
25 Hz	1.329	0.091
40 Hz	3.059	0.067

Even though the dynamic characteristics of the mirrors were determined from sine sweep signals with a limiting frequency of 20 Hz, presented results show that assuming an X-mirror linear phase variation with frequency is applicable even for frequencies higher than 20 Hz. With this scanning system, acceptable TLDV results could now be captured.

3. Correlation between 3DPT and TLDV

3.1 Method and test setup

Figure 8 depicts the experimental setup used to correlate the 3DPT and TLDV displacement measurements. The setup consisted of a five blade planar disk (blisk) driven by a speed controlled motor. Two Photron FASTCAM SA4 cameras were placed on either side of the scanning head, on a different test bench from that on which the blisk and the motor were mounted. Two LED lights were used to improve the illumination of the blisk and hence the quality of the images captured using the

SA4 cameras. The test setup was equipped with two electromagnets for lateral excitation of the blades.

The cameras were used to track the LDV laser dot focused on one of the blades as it was laterally excited while rotating. They were set to record at 3600 FPS. With an on-board camera memory of approximately 16 GB, 10918 images could be recorded at maximum resolution (1024×1024 pixels), thus a total recording time of 3.03 s. FASTCAM software was used to control the cameras. As can be noted in Figure 9, a retro-reflective tape was attached to the blades to ensure that a distinct circular laser dot was captured using the cameras. A Nikon AF-S Nikko 70-200mm 1:2.8G ED VR II lens with a constant maximum aperture of f/2.8 was used. At a set focal length of 70 mm, the starburst pattern that could result from imperfections on the lens surface or aperture diffraction could be adequately reduced. In the presence of a considerable changing starburst pattern, the photogrammetry software will have difficulties identifying the circular laser dot in the images, and this can significantly affect the quality of the registered displacement profiles.

The scanning head used for the LDV had a sensitivity of 5.12 mm/V. While LDVs are usually used to capture velocities through transformation of a Doppler frequency shift into a voltage which is proportional to velocity, the PSV 300 can directly capture displacements by decoding the phase shift [30]. Since the PSV300 results being captured were to be correlated to 3DPT displacements measurements, it was chosen to measure displacement with the PSV300 to avoid integration errors.

The speed of the motor was controlled by a DC voltage supplied to the motor control unit using a NI cDAQ-9178 data acquisition card. Shaft rotational speed was continuously measured using a shaft encoder and was synchronized to the laser beam scanning frequency.

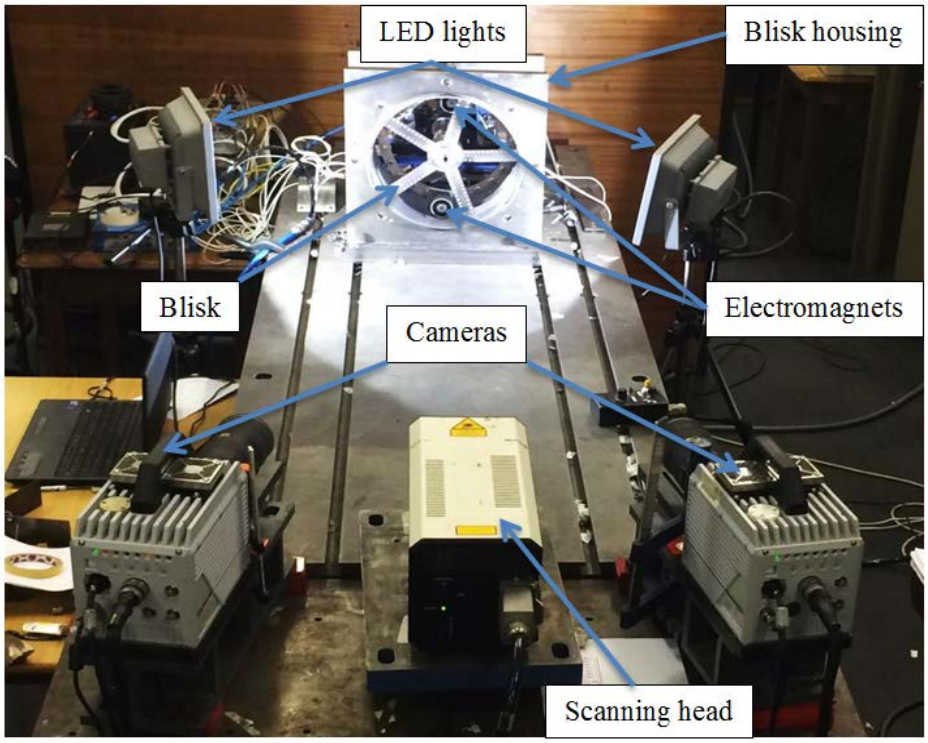

Figure 8: TLDV and 3DPT experimental setup

A shutter speed of 1/8000 of a second was set for the cameras. Static points, with reference to which, displacements were calculated in PONTOS were added to the bladed disk (blisk) housing. Additional

analysis points were added to the blisk as at least three points are required for analysis by the software. Figure 9 shows the setup of the blisk.

The same trigger signal was used to initiate data capturing of TLDV displacement voltage signals and to initiate image capturing with the SA4 cameras.

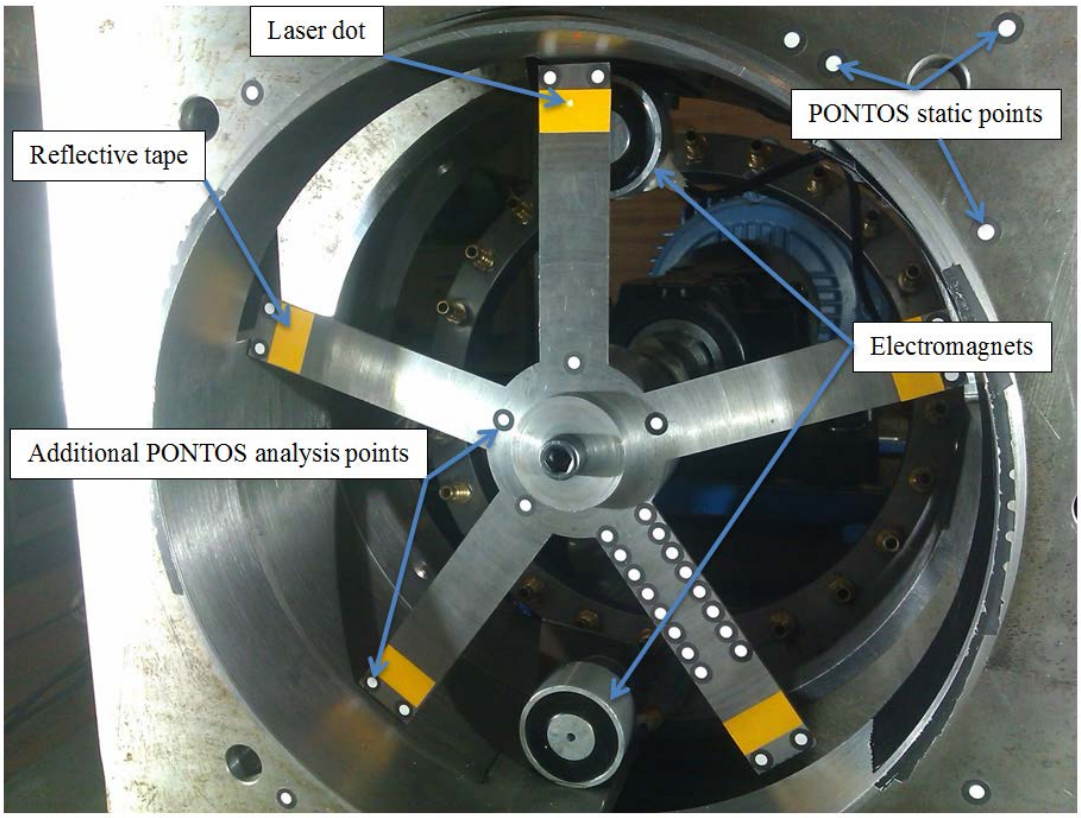

Figure 9: Blisk setup

The investigation was conducted for the scenario where the blades were being excited with two electromagnets, and at a rotational speed of 16.53 Hz. From a visualization of the blisk response using 3DPT software (PONTOS), it was noted that at this rotational speed the blisk ODS was similar to the blisk's first bending mode. A Campbell diagram developed from a finite element (FE) analysis of a model updated numerical representation of the blisk estimated the natural frequency for this first bending mode to be 132 Hz.

3.2 Results and discussion

3DPT and TLDV results were captured on the blisk for periods of 2.3 s. A low frequency sinusoidal component was observed in both of the out-of-plane blade displacement profiles, as is apparent in Figures 10 and 11.

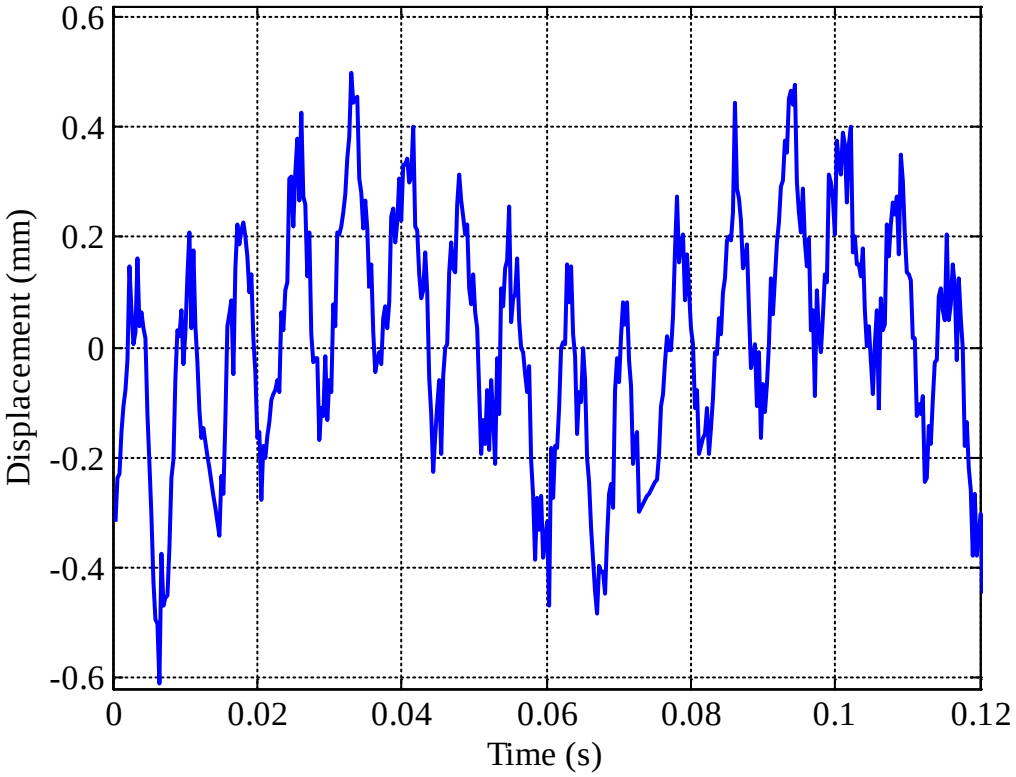

Figure 10: 3DPT time domain raw data

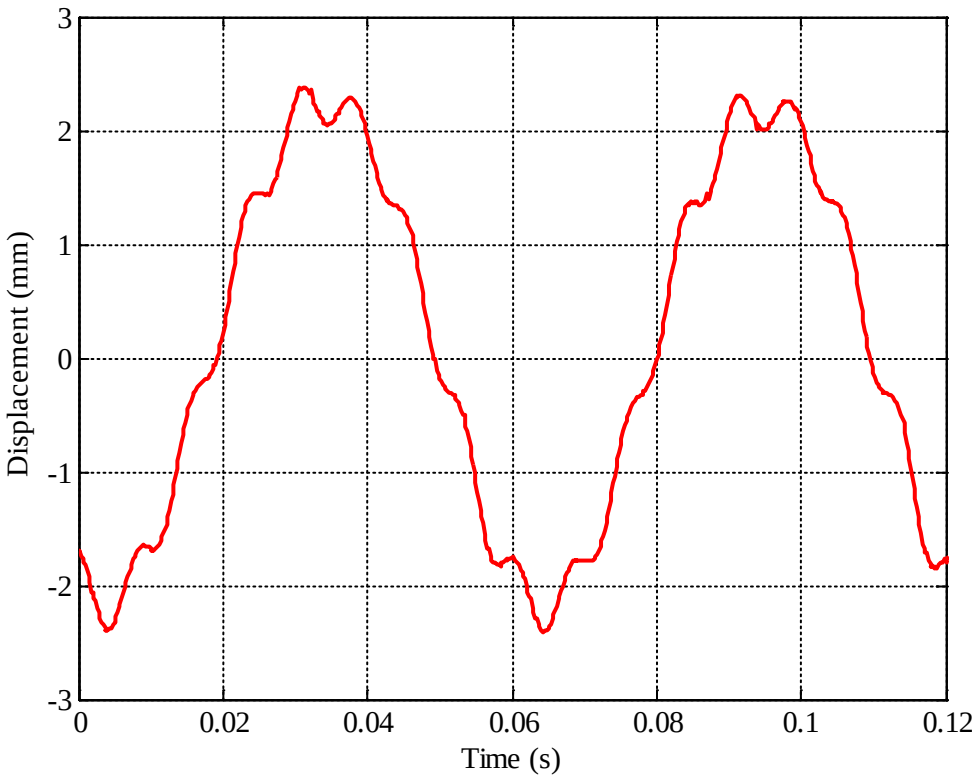

Figure 11: TLDV time domain raw data

An investigation in the frequency domain was subsequently conducted. It was observed that this low frequency component was at 16.53 Hz, corresponding to the rotational frequency of the blisk, which is also 16.53 Hz. Thus this translational misalignment effect completely masks the actual out-of-plane blade vibrations and had to be filtered out before time domain comparisons of the measurements could be conducted.

To correlate 3DPT and TLDV results in the time domain, low frequency components due to misalignment were filtered out using a 10th order digital Butterworth highpass filter. The lower cutoff frequency was set at 50 Hz, which is just above the third rotor speed frequency harmonic of 49.6 Hz. The filter was implemented in a zero-phase forward and reverse digital infinite impulse response (IIR) format to avoid phase distortion. Results in Figure 12 were obtained.

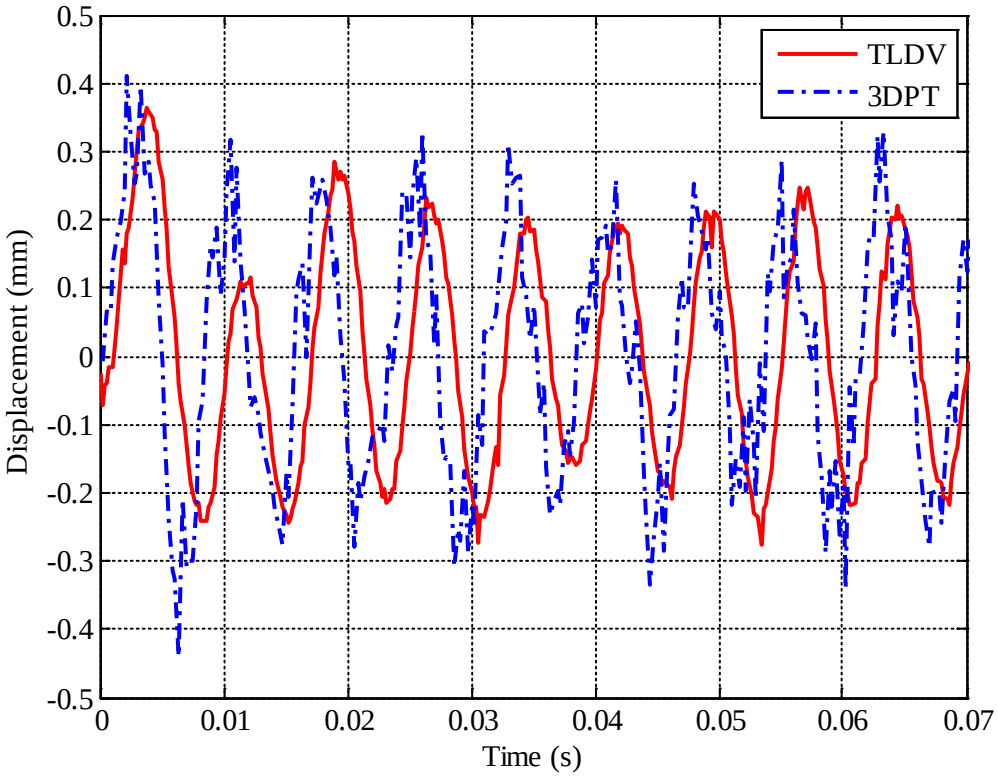

Figure 12: Filtered time domain correlation between 3DPT and TLDV

From Figure 12, a time delay of approximately 2 ms can be observed for the 3DPT measurements. Since a forward and reverse filtering approach was employed to filter out misalignment, no phase distortion resulting from the filtering process was expected. When post-processing the photogrammetry data, the first image cannot be considered to have been taken at time t = 0 s. Some delay from system response to external trigger (T_{trig}), the exposure time (T_{exp}) and the inter-frame delay (T_{int}) is expected, and it has to be compensated for. Thus the total delay in the system (T_{delay}) can be calculated according to Equation (8).

$$T_{delay} = T_{trig} + T_{exp} + T_{int} \tag{8}$$

For Photron SA4 cameras a general trigger response delay is documented as 45 ns, and the sensor readout as 667 ns [31]. As mentioned previously, a shutter speed of 1/8000 s was set for the cameras, implying that the exposure time was 0.125 ms. Thus a total delay of 0.126 ms was to be expected. This however leaves a delay of about 1.874 ms in the 3DPT measurements (6.747 frames).

The exposure time is accurately determined from the specified shutter speed. Since it was possible to sample at 3600 FPS, it means that the system could transfer the images from the sensor to storage (inter-frame delay) fast enough to avoid interference with camera image sampling rate. Thus the most significant delay results from a trigger response time of the used camera system being much longer than the documented value. A further investigation to check whether the hardware trigger response time is actually longer than the documented value will have to be conducted.

For better time domain correlations between the two techniques, the Photron SA4 cameras capability to simultaneously record voltage signals whilst capturing the images can be employed. Signals can be recorded at a sampling rate that corresponds to the set camera frame rate, implying that each image will have a voltage value that corresponds to it. Time delays between the two techniques will thus be avoided. The resolution of the measured TLDV signal profiles would however be limited to the cameras' sampling rate (3600 FPS in this case). As TLDV was being considered as a validating measurement technique to 3DPT recordings, higher sampling rates were needed for improved signal-to-noise Ratio (SNR) and thus better TLDV recordings. Thus a separate system was used to capture TLDV readings, and not the cameras.

Figure 13 shows the displacement profiles after compensation for the photogrammetry system delay.

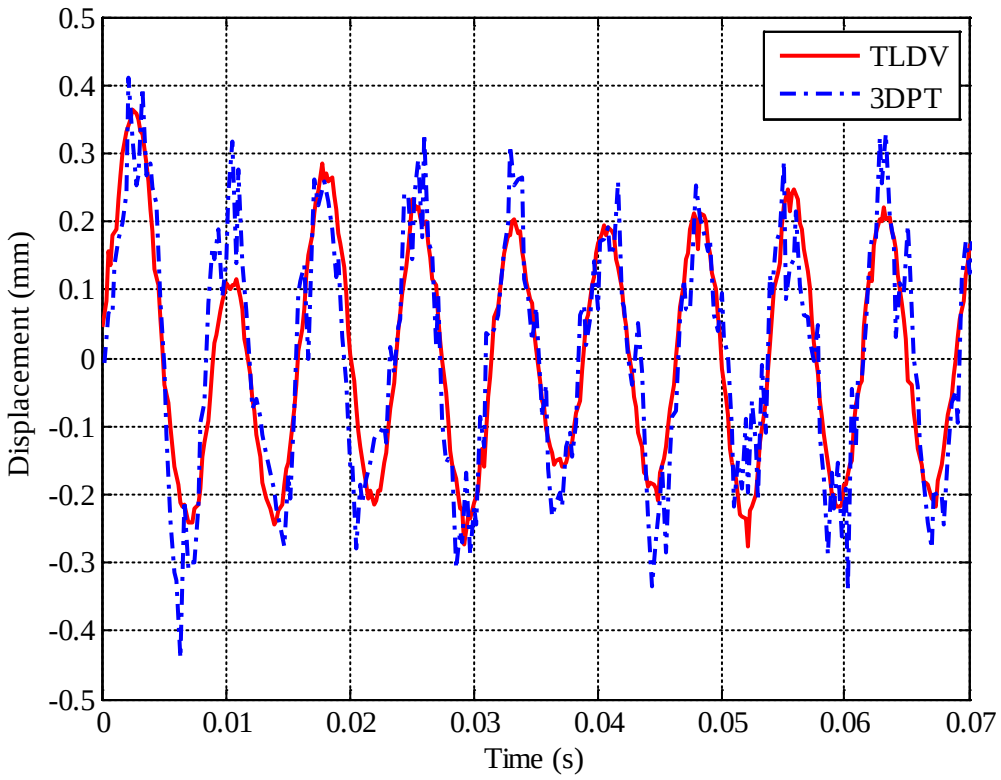

Figure 13: Filtered time domain correlation between 3DPT and TLDV (trigger response compensation)

Figure 13 indicates that the captured displacements were similar to each other, with some amplitude variations mostly from the noise in the 3DPT measurements. For these small amplitude measurements (less than half of a millimetre) the noise can be reduced by using a higher frame rate, which enhances the tracking capability of the photogrammetry software. When using high speed cameras, an increased frame rate however comes at the cost of a reduced allowable maximum camera resolution. For the entire blisk to be in the field of view (FOV) of both cameras, the two cameras would then have to be positioned further away from the blisk. The cameras would also have to be further away from each

other for better system calibration and therefore accurate capture of out-of-plane motion. In an investigation similar to this one where the blisk is inside a housing, much more space is required to ensure that cameras positioned further away are able to capture the blade tips without the housing getting in the way. Thus in this investigation, a compromise had to be made on the frame rate due to space limitations.

Figure 14 shows the correlation between the 3DPT and TLDV displacement profiles in the frequency domain.

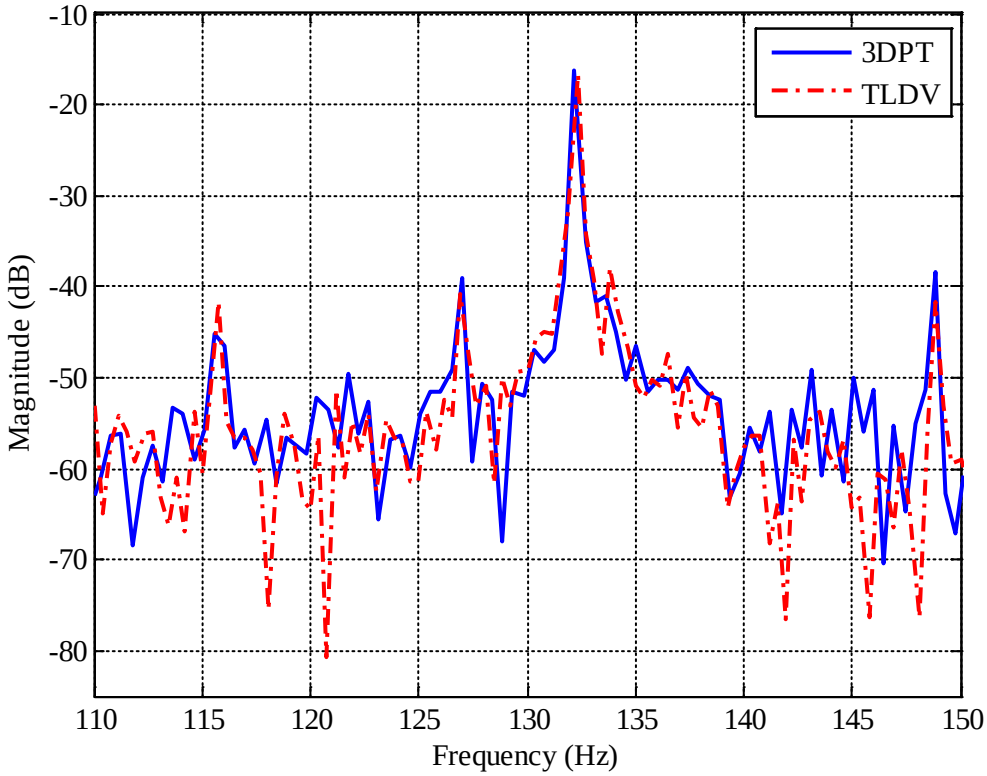

Figure 14: Filtered frequency domain correlation between 3DPT and TLDV

From the results presented in Figure 14, it can be observed that the RMS magnitude peaks for both 3DPT and TLDV occur at the same frequencies in the frequency range of interest. At the out-of-plane blade vibration frequency (132.2 Hz), good correlation between the 3DPT and TLDV systems can also be observed. In the correlation conducted between photogrammetry and accelerometer readings [23], the discrepancies noticed in the frequency domain were attributed to mass loading, accelerometer cross-axis sensitivity, and also the optical system noise floor. The errors associated with the contact measurement technique were eliminated in this investigation, but from the results it can be concluded that there is indeed slight variations between photogrammetry and TLDV. There is 2.5 % maximum difference in magnitude and 0.076 % difference in frequency at the frequency peaks (percentages calculated with reference to TLDV measurements).

The investigation conducted here does differ from the one presented in literature in terms of rotor speed, which influences the magnitude of the accelerometer cross-axis sensitivity error, and blade size which influences the magnitude of the error due to mass loading. However, in comparison to the correlation between 3DPT and accelerometers presented in literature, it is apparent that eliminating contact technique errors does not significantly improve the correlation between 3DPT and other techniques. Thus the errors in the system due to the optical system noise floor seem to contribute more to the discrepancies observed between the various measurement techniques. The effect of mass loading and accelerometer cross-axis sensitivity is thus expected to be more influential in less rigid

structures rotating at much higher rotor speeds. Quantification of the magnitudes of the contact technique errors and determination of cases where accelerometers become unacceptably inaccurate will therefore require further investigations.

Despite the slight variations, the results presented in Figures 13 and 14 illustrate good correlation between 3DPT and TLDV. The optical system noise floor of the photogrammetry system can be considered small enough for the technique to be employed for accurate full-field measurements. Thus a good understanding of the vibration of rotating blades can be captured using photogrammetry.

4. Conclusions and further investigations

A TLDV system was successfully implemented to track a specific point on a blade of a rotating blisk. This made it possible to capture the out-of-plane motion of that specific point with a laser vibrometer. With this capability, the integrity of photogrammetry results could now be investigated by analysing the correlation between 3DPT measurements and another non-contact vibration measurement technique. Thus irregularities attributed to the use of a contact method for validating 3DPT measurements could be eliminated and the applicability of photogrammetry for investigating dynamics of turbomachines analysed using a more reliable and superior approach.

The blade out-of-plane displacement profiles captured using 3DPT and TLDV were successfully compared in both the time and frequency domain. After successful compensation for errors introduced by translational misalignments between the instrumentation and the blisk, and also the photogrammetry system delay, good correlation was observed in the time domain. In the frequency domain, good correlation in the frequency range of interest was also noticed. Contact methods based errors were completely eliminated. It was shown that for generally rigid structures rotating at relatively low speeds, the optical system noise floor contribute more to the discrepancies between 3DPT and accelerometer readings than the mass loading and cross-axis sensitivity.

The good correlation between 3DPT and TLDV established using an approach where most sources of errors eliminated illustrated that photogrammetry can be reliably used as a full-field non-contact technique for analysing online dynamics of turbomachines. While 3DPT and TLDV are largely limited to a laboratory environment, they are useful for validating other more robust non-contact techniques for industrial use. These include blade tip timing and the use of continuous microwave proximity sensors. Since there are applications where accelerometers and strain gauges are better suited for dynamic analysis of structures, further investigations will involve quantifying the errors due to mass loading, telemetry systems noise, and transducer cross-axis sensitivity.

5. Acknowledgements

The authors would like to thank to Mr Dave Reinecke and the CSIR DPSS Landward Sciences division for making their cameras available to us.

6. Nomenclature

A : Area

C_c : Circularity constant

d_s : Scanning mirror separation distance

r_s : Scanning path radius

t : Time

T_{delay} : Time delay

T_{exp} : Exposure time

T_{int} : Inter-frame time

T_{trig} : Trigger time

$\theta_{sx}(t)$: X-mirror scanning angle

$\theta_{sy}(t)$: Y-mirror scanning angle

ϕ_s : Initial phase

φ_{sx} : X-mirror amplitude

φ_{sy} : Y-mirror amplitude

ω : Scanning rotational frequency

Ω_s : Target rotational frequency

7. Abbreviations

3DPT : 3 Dimensional Point Tracking

DIC : Digital Image Correlation

FEA : Finite Element Analysis

FOV : Field Of View

FPS : Frames Per Second

LDV : Laser Doppler Vibrometry

MAC : Modal Assurance Criterion

ODS : Operational Deflection Shape

SNR : Signal-to-Noise Ratio

STLDV : Self Tracking Laser Doppler Vibrometry

TLDV : Tracking Laser Doppler Vibrometry

8. References

[1] P.J. Schubel, R.J. Crossley, E.K.G. Boateng, J.R. Hutchinson, Review of structural health and cure monitoring techniques for large wind turbine blades, Renew. Energy. 51 (2013) 113–123. doi:10.1016/j.renene.2012.08.072.

[2] P. Beauseroy, R. Lengellé, Nonintrusive turbomachine blade vibration measurement system, Mech. Syst. Signal Process. 21 (2007) 1717–1738. doi:10.1016/j.ymssp.2006.07.015.

[3] I.B. Carrington, J.R. Wright, J.E. Cooper, G. Dimitriadis, A comparison of blade tip timing data analysis methods, Proc. Inst. Mech. Eng. Part G J. Aerosp. Eng. 215 (2001) 301–312. doi:10.1243/0954410011533293.

[4] D. Di Maio, D.J. Ewins, Experimental measurements of out-of-plane vibrations of a simple blisk design using Blade Tip Timing and Scanning LDV measurement methods, Mech. Syst. Signal Process. 28 (2012) 517–527. doi:10.1016/j.ymssp.2011.09.018.

[5] G.L. Forbes, R.B. Randall, Estimation of turbine blade natural frequencies from casing

pressure and vibration measurements, Mech. Syst. Signal Process. 36 (2013) 549–561. doi:10.1016/j.ymssp.2012.11.006.

[6] Dantec Dynamics, Appl. Note T-Q-400-Basics-3DCORR-002a-EN, (n.d.). http://www.dantecdynamics.com/docs/products-and-services/dic/T-Q-400-Basics-3DCORR-002a-EN.pdf (accessed December 10, 2014).

[7] M.A. Sutton, J.J. Orteu, H.W. Schreier, Image Correlation for Shape, Motion and Deformation Measurements, Springer Science and Business Media, New York, NY, 2009. doi:10.1007/978-0-387-78747-3.

[8] T. Chu, W. Ranson, M. Sutton, Applications of digital-image-correlation techniques to experimental mechanics, Exp. Mech. (1985) 232–244. http://www.springerlink.com/index/Y002U6538P346776.pdf (accessed July 24, 2013).

[9] R. Wu, Y. Chen, Y. Pan, Q. Wang, D. Zhang, Determination of three-dimensional movement for rotary blades using digital image correlation, Opt. Lasers Eng. 65 (2014) 38–45. doi:10.1016/j.optlaseng.2014.04.020.

[10] B. LeBlanc, C. Niezrecki, P. Avitabile, J. Chen, J. Sherwood, Damage detection and full surface characterization of a wind turbine blade using three-dimensional digital image correlation, Struct. Heal. Monit. 12 (2013) 430–439. doi:10.1177/1475921713506766.

[11] J. Baqersad, C. Niezrecki, P. Avitabile, Full-field dynamic strain prediction on a wind turbine using displacements of optical targets measured by stereophotogrammetry, Mech. Syst. Signal Process. 62-63 (2015) 284–295. doi:10.1016/j.ymssp.2015.03.021.

[12] H.F. Zhou, H.Y. Dou, L.Z. Qin, Y. Chen, Y.Q. Ni, J.M. Ko, A review of full-scale structural testing of wind turbine blades, Renew. Sustain. Energy Rev. 33 (2014) 177–187. doi:10.1016/j.rser.2014.01.087.

[13] J. Winstroth, L. Schoen, B. Ernst, J.R. Seume, Wind turbine rotor blade monitoring using digital image correlation: a comparison to aeroelastic simulations of a multi-megawatt wind turbine, J. Phys. Conf. Ser. 524 (2014) 012064. doi:10.1088/1742-6596/524/1/012064.

[14] M. Ozbek, D.J. Rixen, O. Erne, G. Sanow, Feasibility of monitoring large wind turbines using photogrammetry, Energy. 35 (2010) 4802–4811. doi:10.1016/j.energy.2010.09.008.

[15] R. Wu, Y. Chen, Y. Pan, Q. Wang, D. Zhang, Determination of three-dimensional movement for rotary blades using digital image correlation, Opt. Lasers Eng. 65 (2015) 38–45. doi:10.1016/j.optlaseng.2014.04.020.

[16] M. Ozbek, F. Meng, D.J. Rixen, M.J.L. Van Tooren, Identification of the dynamics of large wind turbines by using photogrammetry, Struct. Dyn. Renew. Energy, Conf. Proc. Soc. Exp. Mech. 1 (2011) 351–359. doi:10.1007/978-1-4419-9716-6.

[17] J.B. Javad, T. Lundstrom, C. Niezrecki, P. Avitabile, Measuring the dynamics of operating helicopter rotors and wind turbines using 3D digital stereophotogrammetry, in: Annu. Forum Proc. - AHS Int., 2013: pp. 2250–2256. http://www.scopus.com/inward/record.url?eid=2-s2.0-84883335554&partnerID=tZOtx3y1.

[18] T. Lundstrom, J. Baqersad, C. Niezrecki, Using high-speed stereophotogrammetry to collect operating data on a Robinson R44 Helicopter, in: R. Allemang, J. De Clerck, C. Niezrecki, A. Wicks (Eds.), Conf. Proc. Soc. Exp. Mech. Ser., Springer New York, New York, NY, 2013: pp. 401–410. doi:10.1007/978-1-4614-6546-1.

[19] L.E. Olson, A.I. Abrego, D.A. Barrows, A.W. Burner, Blade Deflection Measurements of a Full-Scale UH-60A Rotor System, in: Am. Helicopter Soc. Aeromechanics Spec. Conf., 2010: pp. 738–747.

[20] E. Zappa, P. Mazzoleni, A. Matinmanesh, Evaluation and improvement of digital image correlation uncertainty in dynamic conditions, Opt. Lasers Eng. 56 (2014) 140–151. doi:10.1016/j.optlaseng.2013.12.016.

[21] M. Hasanen, P. Saarenrinne, V. Kokko, A New technique for torsional vibration measurements with, in: 26th Int. Congr. Cond. Monit. Diagnostic Eng. Manag., Tampere, 2013: pp. 1–6. http://www.tut.fi/en/about-tut/departments/mechanical-engineering-and-industrial-systems/research/publications/publication/index.htm?id=eJw1jLsOwjAMRb-GLF2AzhlADEgIhITEborVWm3t4jg8_p7Ihe2e-wqQ33EPCRi52px21ZH6Xhb11uECoMhKzOh8Rjajf3qQUnV1FTKTYBQNm47pkee-iSY.

[22] C.N. Mark N. Helfrick, Pawan Pingle, P. Avitabile, Optical Non-contacting Vibration Measurement of Rotating Turbine Blades, in: Imac-Xxviii, Society for Experimental Mechanics Inc., Orlando, Florida USA, 2010: pp. 281–290. doi:10.1007/978-1-4419-9716-6.

[23] C. Warren, C. Niezrecki, P. Avitabile, Optical Non-contacting Vibration Measurement of Rotating Turbine Blades II, in: T. Proulx (Ed.), Soc. Exp. Mech., Springer New York, New York, NY, 2011: pp. 39–44. doi:10.1007/978-1-4419-9716-6.

[24] P. Castellini, M. Martarelli, E. Tomasini, Laser Doppler Vibrometry: Development of advanced solutions answering to technology's needs, Mech. Syst. Signal Process. 20 (2006) 1265–1285. doi:10.1016/j.ymssp.2005.11.015.

[25] A.J. Oberholster, P.S. Heyns, Eulerian laser Doppler vibrometry: Online blade damage identification on a multi-blade test rotor, Mech. Syst. Signal Process. 25 (2011) 344–359. doi:10.1016/j.ymssp.2010.03.007.

[26] A.J. Oberholster, P.S. Heyns, Online condition monitoring of axial-flow turbomachinery blades using rotor-axial Eulerian laser Doppler vibrometry, Mech. Syst. Signal Process. 23 (2009) 1634–1643. doi:10.1016/j.ymssp.2009.01.001.

[27] S. Zucca, D. Di Maio, D.J. Ewins, Measuring the performance of underplatform dampers for turbine blades by rotating laser Doppler Vibrometer, Mech. Syst. Signal Process. 32 (2012) 269–281. doi:10.1016/j.ymssp.2012.05.011.

[28] B.J. Halkon, S.J. Rothberg, Vibration measurements using continuous scanning laser vibrometry: Advanced aspects in rotor applications, Mech. Syst. Signal Process. 20 (2006) 1286–1299. doi:10.1016/j.ymssp.2005.11.009.

[29] D. Di Maio, D.J. Ewins, Applications of continuous tracking SLDV measurement methods to axially symmetric rotating structures using different excitation methods, Mech. Syst. Signal Process. 24 (2010) 3013–3036. doi:10.1016/j.ymssp.2010.06.012.

[30] M. Johansmann, G. Siegmund, M. Pineda, Targeting the Limits of Laser Doppler Vibrometry, (n.d.). http://www.polytec.com/fileadmin/user_uploads/Applications/Data_Storage/Documents/LM_TP_Idema_JP_2005_E.pdf (accessed April 24, 2015).

[31] Photron, FASTCAM SA4 Hardware Manual, (n.d.). http://www.afs.enea.it/apruzzes/Videocamera/fastcam/ (accessed July 1, 2015).